SRI VENKATESWARA INTERNSHIP PROGRAM
FOR RESEARCH IN ACADEMICS
(SRI-VIPRA)
Student Internship

SRI-VIPRA

Project Report of 2025: SVP-2518

"Computational Methods for Differential Equations and Applications"

IQAC
Sri Venkateswara College
University of Delhi
Benito Juarez Road, Dhaula Kuan, New Delhi
New Delhi -110021

SRIVIPRA PROJECT 2025

Title: Computational Methods for Differential Equations and Applications

Name of Mentor: Dr. Swarn Singh **Name of Department: Mathematics** **Designation: Professor**	

List of students under the SRIVIPRA Project

S.No	Photo	Name of the student	Roll number	Course	Signature
1		Parth Jain	1723001	B.Sc.(H) Mathematics	
2		Avi Sehgal	1723090	B.Sc.(H) Mathematics	
3		Anamika Motla	1723131	B.Sc.(H) Mathematics	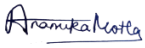
4		Shraddha Chaurasiya	1723123	B.Sc.(H) Mathematics	

5		Devanshi Tandon	1724020	B.Sc.(H) Mathematics	
6		Nikhil Prasad	1723137	B.Sc.(H) Mathematics	
7		Harsh Yadav	1723103	B.Sc.(H) Mathematics	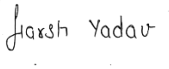
8		Tushti	1724012	B.Sc.(H) Mathematics	
9		Anisha Sahu	1724021	B.Sc.(H) Mathematics	
10		Manoj	1723118	B.Sc.(H) Mathematics	

Signature of Mentor

Certificate of Originality

This is to certify that the aforementioned students from Sri Venkateswara College have participated in the summer project SVP-2518 titled **"Computational Methods for Differential Equations and Applications"**. The participants have carried out the research project work under my guidance and supervision from 1st July, 2025 to 30th September 2025. The work carried out is original and carried out in a hybrid mode.

Signature of Mentor

Acknowledgements

We would like to express our sincere gratitude to Professor Swarn Singh for his invaluable guidance, encouragement, and constant support during our internship on Computational Methods for Differential Equations and Applications at Srivipra. His expertise, insightful suggestions, and constructive feedback played a vital role in deepening our understanding and enhancing the quality of our work.

We also extend our heartfelt thanks to the Srivipra team for providing us with this opportunity, along with the necessary resources and a collaborative environment that greatly enriched our learning experience. This internship has been a rewarding journey, allowing us to strengthen our theoretical knowledge and gain practical exposure to computational methods and their applications.

Lastly, we gratefully acknowledge the support and motivation of our peers and well-wishers throughout the course of this internship.

Table of Contents

Project 1

Epidemic Modelling of COVID-19: Comparative Analysis of SIRD, SEIR, and SEIAQRDT Models

Parth Jain, Avi Sehgal,
Anamika Motla, Shraddha Chaurasiya, Devanshi Tandon

Overview

1 Introduction

The uploaded HTML file contained Python code that works with the dataset (covid_daily_cases.csv) . The purpose of the code is to simulate and evaluate epidemic models (SIRD, SEIR, SEIAQRDT) and compare their predictions with actual COVID-19 data.
This report provides a clear walkthrough of what the code does, presents sample outputs generated using the Indian dataset, includes figures for clarity, and provides detailed observations.

2 What the Code Does ?

The extracted code from the HTML follows these main steps:

1. **Load Dataset:** Reads the COVID-19 daily cases dataset (covid_daily_cases.csv). This dataset contains over 500,000 rows with entries for multiple countries, including India.
2. **Filter by Country:** Extracts the relevant time series for a selected country (India in this case) for analysis.
3. **Define Models:** Implements three key epidemic models:
   - **SIRD** (Susceptible – Infected – Recovered – Dead)
   - **SEIR** (Susceptible – Exposed – Infected – Recovered)
   - **SEIAQRDT** (an extended model including Asymptomatic (A), Quarantine (Q), Protected (T), Recovered (R) and Deceased (D)).
4. **Simulate Dynamics:** Runs numerical simulations of these models over the chosen period to estimate how cases evolve over time.
5. **Compute Errors:** Calculates the relative error (%) between the simulated model predictions and observed data points at the last modelled day to assess accuracy.
6. **Relative Errors at Last Modelled Day (%):**

Model	Relative Error (%)
SIRD	120.51%
SEIR	126.25%
SEIAQRDT	61.48%

7. **Visualize Results:** Produces multiple figures including daily new cases, 7-day moving averages, and cumulative counts. These figures help compare actual epidemic curves with the model-generated predictions.

3 Sample Outputs (India Example)

Using India as a case study, the dataset was processed to compute daily cases (per million), a 7-day moving average, and a cumulative running total.

Key Results

- Number of days in dataset: 2056
- Date range: starting from 2020-01-02
- Total sum of daily values (per million): 31,609.9
- Mean daily cases (per million): 15.38
- Maximum daily value (per million): 274.50 on 2021-09-05

Figures (Outputs Generated by the Code)

- *Daily new confirmed cases per million (India)* – shows raw trend over 2056 days, highlighting multiple COVID-19 waves.
- *7-day moving average (India)* – smooths fluctuations to show clearer epidemic peaks, particularly during the Delta and Omicron waves.
- *Cumulative cases per million (India)* – steadily rising line showing the long-term impact of the pandemic, reflecting overall case accumulation.
- *Model Prediction vs Actual Data Plots* – overlays model-predicted curves (SIRD, SEIR, SEIAQRDT) with real data, allowing visual comparison of fit quality.

COVID-19 Model Predictions vs Actual Cumulative Cases

(The provided figure overlays the actual cumulative cases (black line) with the predicted cumulative cases from SIRD, SEIR, and SEIAQRDT models.)

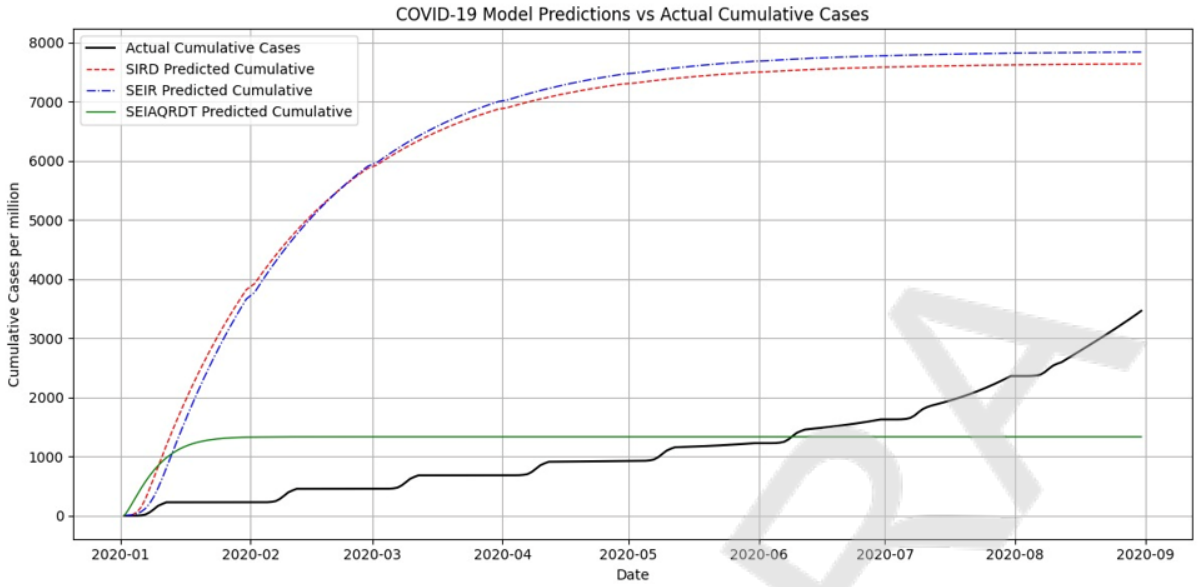

4 Conclusion

The uploaded code effectively demonstrates how epidemic models can be simulated and compared against real COVID-19 data.
The Indian dataset results show realistic epidemic trends, including the Delta wave peak in September 2021. With the inclusion of figures, the results become easier to interpret and visually confirm.
The models provide a useful foundation for understanding and predicting epidemic dynamics, giving insights into infection growth, epidemic peaks, and cumulative impacts over time.

References

1. Kamrujjaman M, Mahmud MS, Islam MS (2020) Coronavirus outbreak, and the mathematical growth map of COVID-19. *Annu Res Rev Biol* 35(1):72–78. https://doi.org/10.9734/arrb/2020/v35i130182

2. WHO. Coronavirus disease (COVID-19) pandemic.
Available from:
https://www.who.int/emergencies/diseases/novel-coronavirus-2019. Accessed 6 July 2020.

3. Covid19 India. Available from: https://www.covid19india.org/. Accessed 6 July 2020.

4. Giordano G, Blanchini F, Bruno R, Colaneri P, Di Filippo A, Di Matteo A, Colaneri M (2020) Modelling the COVID-19 epidemic and implementation of population-wide interventions in Italy. *Nat Med* 26:855–860. https://doi.org/10.1038/s41591-020-0883-7

5. Wang Y, Wang Y, Chen Y, Qin Q (2020) Unique epidemiological and clinical features of the emerging 2019 novel coronavirus pneumonia (COVID-19) implicate special control measures. *J Med Virol* 92(6):568–576.

6. Zou L, Ruan F, Huang M, Liang L, Huang H, Hong Z, Yu J, Kang M, Song Y, Xia J, Guo Q, Song T, He J, Yen HL, Peiris M, Wu J (2020) SARS-CoV-2 viral load in upper respiratory specimens of infected patients. *N Engl J Med* 382(12):1177–1179.

7. Anderson RM, May RM (1992) *Infectious diseases of humans: dynamics and control*. Oxford University Press Inc., New York.

8. Diekmann O, Heesterbeek JAP (2000) *Mathematical epidemiology of infectious diseases: model building, analysis and interpretation*. John Wiley and Sons, Chichester.

9. Hethcote H (2000) The mathematics of infectious diseases. *SIAM Rev* 42(4):599–653.

10. Brauer F, Chavez CC (2012) *Mathematical models in population biology and epidemiology*. Springer, New York, NY. https://doi.org/10.1007/978-1-4614-1686-9

11. Kermack WO, McKendrick AG (1927) A contribution to the mathematical theory of epidemics. *Proc. Royal Society of London. Series A* 115(772):700–721.

12. Lin Q, Zhao S, Gao D, Lou Y, Yang S, Musa S, Wang M, Cai Y, Wang W, Yang L, He D (2020) A conceptual model for the outbreak of Coronavirus disease 2019 (COVID-19) in Wuhan, China with individual reaction and governmental action. *Int J Infect Dis* 93:211–216.

13. Prem K, Liu Y, Russell TW, Kucharski AJ, Eggo RM, Davies N, Flasche S, Clifford S, Pearson CAB, Munday JD, Abbott S, Gibbs H, Rosello A, Quilty BJ, Jombart T, Sun F, Diamond C, Gimma A, Zandvoort KV, Funk S, Jarvis CI, Edmunds WJ, Bosse NI, Hellewell J, Jit M, Klepac P (2020) The effect of control strategies to reduce social mixing on outcomes of the COVID-19 epidemic in Wuhan, China: a modelling study. *The Lancet Public Health* 5(5). https://doi.org/10.1016/S2468-2667(20)30073-6

14. Peng L, Yang W, Zhang D, Zhuge C, Hong L (2020) Epidemic analysis of COVID-19 in China by dynamical modeling. *arXiv preprint* arXiv:.06563.

15. López L, Rodó X (2020) A modified SEIR model to predict the COVID-19 outbreak in Spain and Italy: simulating control scenarios and multi-scale epidemics. Available at SSRN: https://doi.org/10.2139/ssrn.3576802

16. Cantó B, Coll C, Sánchez E (2017) Estimation of parameters in a structured SIR model. *Adv Diff Eqs* 2017(1):33.

17. Chen Y, Cheng J, Jiang Y, Liu K (2020) A time delay dynamical model for outbreak of 2019-nCoV and the parameter identification. *J Inverse Ill-Posed Prob* 28(2):243–250.

18. Ma S, Xia Y (2008) *Mathematical understanding of infectious disease dynamics*, Lecture Notes Series, Institute for Mathematical Sciences, National University of Singapore. World Scientific 16:240. https://doi.org/10.1142/7020

19. Liu C, Ding G, Gong J, Wang L, Cheng K, Zhang D (2004) Studies on mathematical models for SARS outbreak prediction and warning. *Chin Sci Bull* 49(21):2245–2251.

20. Zareie B, Roshani A, Mansournia MA, Rasouli MA, Moradi G (2020) A model for COVID-19 prediction in Iran based on China parameters. *J Arch Iran Med* 23(4):244–248.

21. Zhang LJ, Wang FC, Zhuang XQ, et al. (2019) Global stability analysis on one type of SEIR epidemic model with floating population. *J Institute Dis Prev* 21(2):78–81.

22. Ru-Guo F, Wang YB, Luo M, et al. (2020) SEIR-based novel pneumonia transmission model and inflection point prediction analysis. *J Univ Electron Sci Technol China* 49:1–6.

23. Zhou T, Liu Q, Yang Z, Liao J, Yang K, Bai W, Lu X, Zhang W (2020) Preliminary prediction of the basic reproduction number of the Wuhan novel coronavirus 2019-nCoV. *J Evidence-Based Med* 13(1):3–7.

Project 2

Numerical Simulation of 1D Heat Transfer in a Composite Rod using the Crank–Nicolson Method

Nikhil Prasad, Harsh Yadav, Tushti, Anisha Sahu

Abstract

This report presents a numerical simulation of transient heat transfer in a one-dimensional composite rod composed of three distinct materials. The conservative form of the heat equation was solved using the Crank-Nicolson method. We used a harmonic mean for the thermal conductivity to determine the physical precision at the material interfaces. A dual convergence criterion was implemented that requires both thermal stability and flux continuity to successfully distinguish between physically valid and invalid results. The model was tested by comparing its steady state results to an exact analytical solution derived from the thermal resistance method. The simulation demonstrates that the Crank-Nicolson scheme is highly accurate for small time steps (Δt). However, for larger time steps, the method produces non-physical oscillations, leading to significant errors and a loss of flux continuity. These findings highlight the critical difference between the numerical stability of a method and its ability to produce physically accurate results.

Overview

*

5 Introduction

We are using the Crank-Nicolson method[1], a popular and unconditionally stable scheme to solve time-dependent problems. It calculates the heat flow using the average of the temperature in the present time step and the temperature at the next time step. We will use this method to run the simulation of heat transfer in a 1D rod made up of three distinct materials. Our primary objective is to make a reliable simulator for our system using the Crank-Nicolson method.But before we begin any further we will set up our problem followed by derivation of the Crank-Nicolson scheme, and the physical system under study is a one-dimensional composite rod of total length $L = 1.0\,\mathrm{m}$, consisting of three distinct material segments joined end-to-end without any gaps:

- Material A: occupies the interval $[0, 0.3]\,\mathrm{m}$, with thermal conductivity $k_A = 10.0\,\mathrm{W/mK}$,
- Material B: occupies the interval $[0.3, 0.7]\,\mathrm{m}$, with thermal conductivity $k_B = 1.0\,\mathrm{W/mK}$,
- Material C: occupies the interval $[0.7, 1.0]\,\mathrm{m}$, with thermal conductivity $k_C = 5.0\,\mathrm{W/mK}$.

For simplicity, the product of density and specific heat was taken as constant,

$$\rho c_p = 1.0\,\mathrm{J/(m^3K)}.$$

5.1 Boundary and Initial Conditions

Dirichlet boundary conditions were applied at both ends of the rod:

$$T(0,t) = 100^\circ\mathrm{C}, \qquad T(L,t) = 20^\circ\mathrm{C}.$$

The initial condition inside the rod was uniform:

$$T(x,0) = 20^\circ\mathrm{C}, \qquad 0 < x < L.$$

5.2 Discretization Parameters

The spatial domain was discretized into $N_x = 101$ uniformly spaced grid points, giving a spacing of

$$\Delta x = \frac{L}{N_x - 1} = 0.01\,\mathrm{m}.$$

The temporal domain was advanced using several different time steps to study the stability and accuracy of the scheme:

$$\Delta t \in \{0.0005,\ 0.005,\ 0.05,\ 0.1,\ 0.5\}\,\text{s}.$$

6 Derivation of the Crank–Nicolson Method

We consider the one-dimensional transient heat conduction equation in conservative form:

$$\frac{\partial T}{\partial t} = \alpha \frac{\partial^2 T}{\partial x^2}, \qquad x \in [0, L],\ t > 0 \tag{1}$$

where $T(x,t)$ is the temperature field and $\alpha = \frac{k}{\rho c_p}$ is the thermal diffusivity.

6.1 Spatial Discretization

Divide the rod into N grid points with spacing $\Delta x = \frac{L}{N-1}$. Let T_i^n denote the numerical approximation to $T(x_i, t^n)$, where $x_i = i\Delta x$ and $t^n = n\Delta t$.

The second derivative is approximated using the central difference:

$$\left.\frac{\partial^2 T}{\partial x^2}\right|_{x_i,t^n} \approx \frac{T_{i+1}^n - 2T_i^n + T_{i-1}^n}{(\Delta x)^2}. \tag{2}$$

6.2 Time Discretization

The time derivative is approximated using a finite difference:

$$\left.\frac{\partial T}{\partial t}\right|_{x_i} \approx \frac{T_i^{n+1} - T_i^n}{\Delta t}. \tag{3}$$

The Crank–Nicolson method applies the trapezoidal rule in time, averaging the spatial operator at times n and $n+1$:

$$\frac{T_i^{n+1} - T_i^n}{\Delta t} = \frac{\alpha}{2}\left[\frac{T_{i+1}^n - 2T_i^n + T_{i-1}^n}{(\Delta x)^2} + \frac{T_{i+1}^{n+1} - 2T_i^{n+1} + T_{i-1}^{n+1}}{(\Delta x)^2}\right]. \tag{4}$$

6.3 Rearranging

Introduce the diffusion number:

$$r = \frac{\alpha \Delta t}{2(\Delta x)^2}. \tag{5}$$

Substituting into the scheme gives:

$$-rT_{i-1}^{n+1} + (1+2r)T_i^{n+1} - rT_{i+1}^{n+1} = rT_{i-1}^n + (1-2r)T_i^n + rT_{i+1}^n. \tag{6}$$

6.4 Matrix Form

For all interior nodes, this yields a tridiagonal system:

$$\mathbf{A}\,\mathbf{T}^{n+1} \;=\; \mathbf{B}\,\mathbf{T}^{n}, \tag{7}$$

where:

- $\mathbf{A}$ and $\mathbf{B}$ are tridiagonal matrices with entries depending on r,
- $\mathbf{T}^n = [T_1^n, T_2^n, \ldots, T_{N-2}^n]^T$ contains interior temperatures.

6.5 Harmonic Mean for Interface Conductivity

Since we have taken a rod made of three distinct materials, we have different conductivity values k, which are not uniform. They change at the interfaces between two materials. We used the harmonic mean for the thermal conductivity at the interfaces of two different materials. Using this approach, there is no violation of energy conservation at the boundaries of different materials and flux continuity is ensured[2]. The general harmonic mean formula for two conductivities k_L and k_R (at the left and right side of an interface) is:

$$k_{\text{face}} = \frac{2k_L k_R}{k_L + k_R}, \tag{8}$$

6.6 Exact Analytical Solution

To test our numerical results, we obtained the analytical solution using the thermal resistance method. Each segment of material in the rod is treated as a thermal resistor with resistance.

$$R = \frac{L}{k}, \tag{9}$$

where L is the length of the segment and k is its thermal conductivity. For the three segments of the composite rod, we have

$$R_A = \frac{L_A}{k_A}, \qquad R_B = \frac{L_B}{k_B}, \qquad R_C = \frac{L_C}{k_C}. \tag{10}$$

The total resistance of the rod is therefore

$$R_{\text{total}} = R_A + R_B + R_C. \tag{11}$$

The exact steady-state heat flow through the rod is then given by

$$q_{\text{exact}} = \frac{T_{\text{left}} - T_{\text{right}}}{R_{\text{total}}}. \tag{12}$$

Finally, the interface temperatures can be calculated as

$$T_1 = T_{\text{left}} - q_{\text{exact}} R_A, \qquad T_2 = T_{\text{left}} - q_{\text{exact}}(R_A + R_B). \tag{13}$$

For the parameters of this study:

$$L_A = 0.3\,\text{m}, \quad L_B = 0.4\,\text{m}, \quad L_C = 0.3\,\text{m},$$
$$k_A = 10.0\,\text{W/mK}, \quad k_B = 1.0\,\text{W/mK}, \quad k_C = 5.0\,\text{W/mK},$$
$$T_{\text{left}} = 100°\text{C}, \quad T_{\text{right}} = 20°\text{C}.$$

The resistances are the following.

$$R_A = \frac{0.3}{10} = 0.03, \qquad R_B = \frac{0.4}{1} = 0.40, \qquad R_C = \frac{0.3}{5} = 0.06,$$
$$R_{\text{total}} = 0.49.$$

Thus, the analytical heat flow is:

$$q_{\text{exact}} = \frac{100 - 20}{0.49} \approx 163.26,$$

and the interface temperatures are:

$$T_1 = 100 - (163.26)(0.03) \approx 95.10°\text{C}, \qquad T_2 = 100 - (163.26)(0.03 + 0.40) \approx 29.80°\text{C}.$$

These values of q_{exact}, T_1, and T_2 serve as benchmarks for comparison with the results of the numerical simulation.

6.7 Dual Convergence Criteria

Convergence is accepted only if both a numerical and a physical test are satisfied.

a. Temperature criterion Successive temperature fields must change negligibly:

$$\max_i \left| T_i^{n+1} - T_i^n \right| < \varepsilon_{\text{temp}}, \tag{14}$$

with $\varepsilon_{\text{temp}} = 1 \times 10^{-8}$. This value is chosen to be much smaller than actual temperature differences, ensuring accuracy without wasting computation.

b. Flux criterion Flux continuity must hold at all material interfaces. For an interface, left and right fluxes are

$$q_{\text{left}} = -\frac{k_{\text{face}}}{\Delta x}(T_i - T_{i-1}), \qquad q_{\text{right}} = -\frac{k_{\text{face}}}{\Delta x}(T_{i+1} - T_i), \tag{15}$$

and the flux jump is

$$J_{\text{flux}} = q_{\text{right}} - q_{\text{left}}. \tag{16}$$

The requirement is

$$\max_{\text{interfaces}} |J_{\text{flux}}| < \varepsilon_{\text{flux}}, \tag{17}$$

with $\varepsilon_{\text{flux}} = 1 \times 10^{-6}$. This tolerance balances numerical noise and physical consistency.

Why Both Criteria Are Needed Both tests together prevent false convergence: the temperature criterion checks numerical steady state, while the flux criterion enforces energy conservation across material boundaries.

6.8 Software Used: Mathematica

Mathematica (Wolfram Research, Inc.) is a computational software system widely used for both symbolic and numerical mathematics. It provides a rich programming environment for algebraic manipulations, solving differential equations, data visualization, and numerical simulations. In this project, Mathematica was employed to implement the Crank–Nicolson scheme, enforce dual convergence criteria, and generate plots for error analysis [3].

.

7 Output

dt	T(L1)	T(L2)	qAB	qBC	Max Flux Jump	Converged?	Err% T1	Err% T2	Err% qAB	Err% qBC
0.0005	95.097	30.4597	163.432	163.432	9.05×10^{-8}	YES	0.0052608	2.2276	0.102147	0.102143
0.005	95.0969	30.4597	163.471	163.432	0.12195	NO	0.0053739	2.2276	0.125881	0.102145
0.05	101.294	30.4633	257.423	164.326	33.1698	NO	6.51125	2.24001	57.6715	0.649509
0.1	92.1603	29.9549	-203.061	156.974	99.8358	NO	3.09324	0.533727	224.375	3.85351
0.5	29.4523	26.1625	-134.167	86.8312	11.238	NO	69.0308	12.1944	182.177	46.8159

7.1 Interpretation of Results

The conclusions for each tested time step Δt are as follows:

- $\Delta t = 0.0005$**:** The simulation converged successfully. The flux jump was negligible ($\approx 9 \times 10^{-8}$), and both interface temperatures matched the analytical values with less than 2.3% error. This confirms that the Crank–Nicolson scheme is accurate and physically consistent for sufficiently small time steps.
- $\Delta t = 0.005$**:** Although numerically stable, the simulation did not satisfy the flux continuity condition (flux jump ≈ 0.12). Errors in temperatures

and fluxes are still small, but the dual convergence criterion correctly rejected this run, showing the onset of physical inconsistency.

- $\Delta t = 0.05$**:** The flux jump became very large (≈ 33), indicating serious violation of energy conservation at material interfaces. The predicted heat flux q_{AB} deviated by almost 58% from the analytical solution. This demonstrates the non-physical oscillations that arise in Crank–Nicolson with larger time steps.
- $\Delta t = 0.1$**:** The results became even more unreliable. The flux jump exceeded 99, and the heat flux at the AB interface was negative, which is non-physical. Errors in flux reached over 224%, confirming the complete breakdown of physical accuracy.
- $\Delta t = 0.5$**:** The simulation failed entirely. Interface temperatures collapsed to unrealistic values, and the flux errors remained extremely large (above 180%). Although the scheme is formally stable, the solution is meaningless from a physical perspective.

In summary, while the Crank–Nicolson scheme is unconditionally stable, it only produces physically meaningful solutions for sufficiently small Δt. The dual convergence criterion successfully distinguishes between reliable and unreliable cases.

7.2 Interpretation of Error Plots

Four error plots were produced: error in $T(L1)$, error in $T(L2)$, and error in interface fluxes q_{AB} and q_{BC}, each plotted against the time-step Δt on a log–log scale. The main observations is:

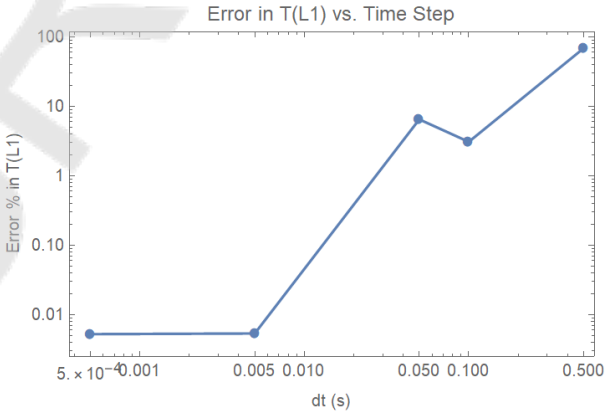

Figure 1: Error in $T(L1)$ vs. Δt (log–log).

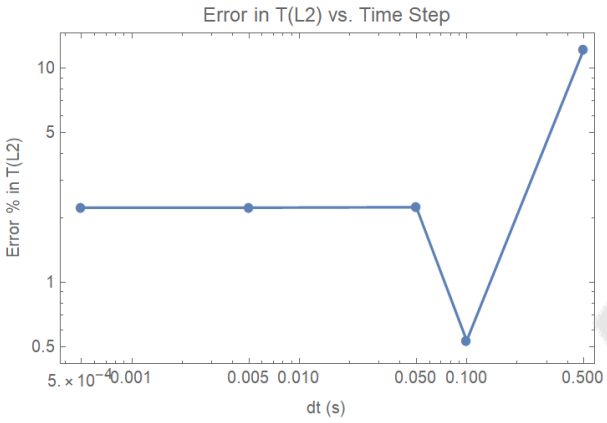

Figure 2: Error in $T(L2)$ vs. Δt (log–log).

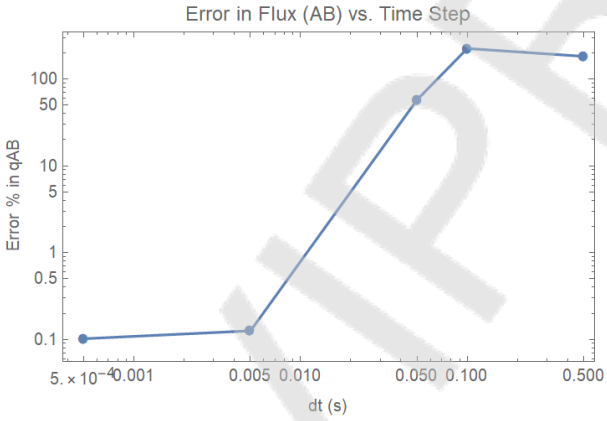

Figure 3: Error in q_{AB} vs. Δt (log–log).

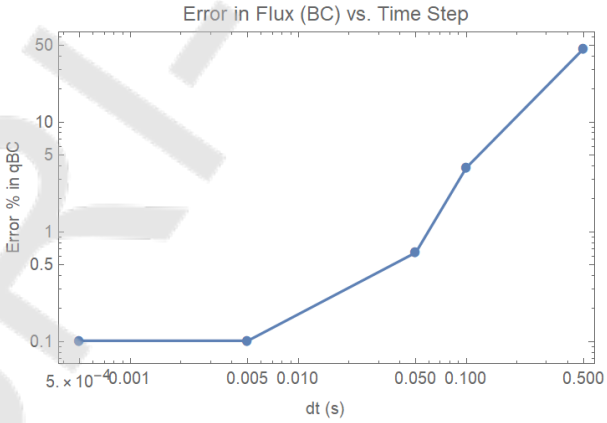

Figure 4: Error in q_{BC} vs. Δt (log–log).

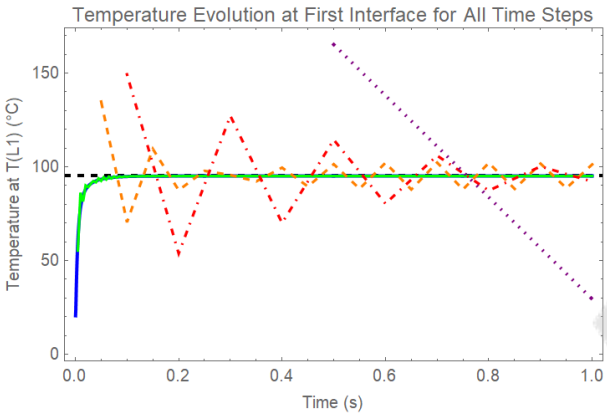

Figure 5: Temperature at $T(L1)$ vs. time for all Δt.

All four plots together demonstrate that decreasing Δt reduces both temperature and flux errors and restores physical flux continuity. The results validate the choice of a strict dual convergence criterion (temperature change tolerance and flux-jump tolerance): it accepts physically-correct runs (e.g. $\Delta t = 5 \times 10^{-4}$) and rejects runs that are numerically stable but physically inconsistent. Practically, one should choose Δt small enough that interface flux errors are acceptable, or alternatively use damping/implicit techniques or finer spatial resolution when conductivity contrasts are large.

8 Conclusion

This project successfully developed and validated a numerical model for one-dimensional heat transfer in a composite rod. The study showed that the Crank–Nicolson scheme, although unconditionally stable in theory for all time-step sizes(Δt), delivers physically reliable results only when sufficiently small time steps are used. With fine temporal discretization, the simulation closely matched the analytical solution, confirming both accuracy and consistency. However, when large time steps were applied, the results exhibited non-physical oscillations, noticeable errors, and a breakdown of flux continuity at the material interfaces, making the outcomes unrealistic. These findings emphasize the important distinction between numerical stability and true physical accuracy. The adoption of a dual-convergence check — particularly the flux-jump diagnostic — proved critical in filtering out solutions that were mathematically stable but physically invalid. This highlights the broader need for physics-based validation techniques when assessing the reliability of numerical simulations.

References

[1] J. Crank and P. Nicolson. A practical method for numerical evaluation of solutions of partial differential equations of the heat-conduction type. *Proceedings of the Cambridge Philosophical Society*, 43(1):50–67, 1947.

[2] Samet Y. Kadioglu, Robert R. Nourgaliev, and Vincent A. Mousseau. A comparative study of the harmonic and arithmetic averaging of diffusion coefficients for non-linear heat conduction problems. In *Proceedings of the 2006 International Conference on Mathematics and Computational Methods Applied to Nuclear Science and Engineering (M&C 2006)*, American Nuclear Society, Monterey, California, USA, April 2006.

[3] Wolfram Research, Inc. Mathematica (version 13.3). Software, 2023. Software system for technical computing. Available at: `https://www.wolfram.com/mathematica`.

Project 3

Explicit Finite Difference Simulation of Heat Conduction in a Circular Plate with Central Heat Source

Manoj

Abstract

The paper provides a numerical study of how heat conducts through a thin circular plate heated at its center by a Gaussian source. The heat equation is written in radial form, assuming the system is axis-symmetric, with Robin boundary conditions at the rim to show cooling by convection and heat loss from the plate surfaces. The plate is treated as very thin, with temperature varying only radially. An explicit finite-difference method is used where the time derivative is approximated using the forward difference approximation and the second-order spatial derivative using the centered difference approximation. The time step follows the Fourier number rule to keep the solution stable. Simulations show that the center heats up the most, the heat moves outward gradually, and the rim stays close to room temperature because of convection. This study shows that the explicit scheme works well for circular domains and gives a basis for future work.

Overview

1 Introduction

Heat transfer is one of the most fundamental processes in nature and technology. It describes the way thermal energy moves from one part of a body to another or from one body to its surroundings. In solids, the main way heat is transferred is by conduction, where energy moves as atoms vibrate and electrons interact with each other [1]. Research on heat conduction has progressed rapidly since Joseph Fourier's work in the early 19th century, when he formulated the heat equation and introduced the Fourier series to study heat conduction in different geometries [2]. Heat conduction in solids follows Fourier's law and the law of energy conservation. These two ideas lay the foundation for the heat equation, which shows how temperature varies within the material. Whenever a solid has a temperature difference within it, heat naturally moves from the hotter regions to the cooler regions.

In order to study conduction with mathematical methods, we need to state the process by which energy enters the system and leaves the system. Such definitions are referred to as boundary conditions. For example, if the edge of the body is kept at a fixed temperature, that is called a Dirichlet condition. If heat cannot pass through the boundary, we call it a Neumann condition. However, in practical terms, heat is always lost from the solid to the surrounding where it is kept. The Robin boundary condition is used here, and it links the heat flux at the surface to the difference between the surface temperature and the temperature of the surrounding medium [1,3].

Many studies have been carried out on heat conduction in different geometries in the past. The simplest cases are a one-dimensional rod and a thin slab, which are studied both numerically and analytically. Rods and slabs are useful starting points for studying heat conduction using numerical methods and analyzing their stability. Previous work on simpler geometries provides useful benchmarks. R. L. Herman (2014) studied the transient heat equation in a one-dimensional rod, solving with numerical methods to investigate temperature distributions under various boundary and initial conditions [4]. In two-dimensional plates, Saraireh et al. have solved heat conduction in square or rectangular geometries subject to convective heat transfer on the surfaces, showing how plate tilt and boundary conditions alter thermal response [5]. Square and rectangular plates have been widely studied with the help of Cartesian coordinates to show spread

to heat in two directions. Furthermore, cylinders have been studied in cases where radial conduction is essential [6]. Peavy (1963) studied steady-state heat conduction in cylinders with internal line heat sources and derived analytical or series solutions for different boundary conditions [7]. In most of these classical studies, the heat source is uniform throughout the material or applied at its boundary.Problems with localized heating, like energy applied at a point or at the center of a plate, have been studied less often, even though they are very important in practice.

The present project focuses on the case of a thin circular plate that receives continuous heat at its center from a Gaussian source. This form of heat source is considered smooth and realistic, and it is widely used to model focused input such as lasers or concentrated energy. At the same time, heat is lost from the rim by convection to the surrounding environment [1], and there is also heat loss from the faces of the plate [6]. This combination creates a physically meaningful problem that involves both heat input and heat loss. The aim of this project is to model and simulate heat conduction in a circular plate with a Gaussian heat source at the center and convective heat loss at the boundary, along with heat loss from the faces. The problem is solved using the explicit finite difference method [8]. The numerical method is applied carefully at all points, including special conditions at the rim and center. The radial governing equation is derived from the heat equation in cylindrical geometry by neglecting the angular dependence, since the plate is thin [9]. Simulations are carried out to study how temperature changes in space with time.

Since analytical solutions for these problems are not possible, numerical methods are required. Therefore, approximation techniques are applied, and the explicit scheme is used in this study. The explicit method is simple to apply and easy to understand, which makes it suitable for an initial computational study on any geometry [8]. This updates the temperature distribution step by step in time, using the values obtained from the previous step. Although this method needs very small time steps to maintain stability [6], it continues to be useful for studying the basic dynamics of heat transfer and for evaluation against advanced methods. To obtain reliable numerical results, the stability of the explicit scheme is analyzed using the classical von Neumann method. This analysis gives the well-known stability condition written in terms of the Fourier number, which is then used as a guideline for selecting appropriate spatial and time step sizes in heat conduction simulations [10, 11].

The present study is not only a numerical simulation, but also illustrates a model problem for several real systems. A similar situation exists in disc brakes, where the center is the most heated and heat is lost outward [12]. In electronic devices, circuit boards often show small central hot spots near the chips, with heat spreading radially outward in a similar way [13]. In materials science, lasers commonly use a Gaussian-type source to heat thin sheets [1], which are comparable to the model studied here. Even in biomedical applications, focused ultrasound and laser therapies follow the same type of model [14]. Thus, although several assumptions are used, the study still connects closely with real-world applications.

This work also lays the foundation for further research. The explicit scheme is simple to use and conditionally stable, but it becomes inefficient for long-term simulations. This limitation motivates the use of unconditionally stable methods, such as the Crank–Nicolson scheme, which can be explored in future studies [15]. Other ways to improve the model are by including the thickness of the plate, studying angular variations, allowing material properties to change with temperature, or testing different methods on the same geometry. With these changes, the model would better match real-life cases and support real engineering analysis.

2 Mathematical Formulation

2.1 Governing Equation

The governing equation of the problem is obtained by combining Fourier's law, Newton's law of cooling, and the law of energy conservation in the radial equation. The plate is assumed to be thin and the temperature is taken as a function of the radial coordinate r and the time t. The resulting equations are given below.

$$
\begin{aligned}
u_t &= \mathcal{D}[u] + \mathcal{S}(r,u), \qquad 0 \le r \le R,\ t > 0, \\
\mathcal{D}[u] &= \alpha \left(u_{rr} + \frac{1}{r} u_r \right), \\
\mathcal{S}(r,u) &= \frac{Q_0 e^{-\beta r^2}}{\rho c s} - \frac{2h}{\rho c s} (u - T_\infty).
\end{aligned}
$$

where

Symbol	Description
$u(r,t)$	Temperature at radial position r and time t (K)
R	Radius of the circular plate (m)
α	Thermal diffusivity, $\alpha = k/(\rho c)$ (m^2/s)
k	Thermal conductivity of the material (W/mK)
$Q_0 e^{-\beta r^2}$	Gaussian heat source
Q_0	Source strength or maximum heat generation at the centre ($\mathrm{W/m}^3$)
β	Spread parameter of the Gaussian profile, controlling how localised the source is (m^{-2})
h	Convection heat transfer coefficient ($\mathrm{W/m}^2\mathrm{K}$)
s	Plate thickness (m)
ρ	Density of the material ($\mathrm{kg/m}^3$)
c	Specific heat capacity (J/kgK)
T_∞	Ambient temperature (K)

Table 1: List of symbols used in the mathematical model.

The governing equation contains the radial diffusion terms arising from cylindrical symmetry, along with a face-loss term that represents convective cooling. The coefficient of two in the loss term is included because both faces of the thin plate are exposed to air. These adjustments ensure that both the symmetry of the geometry and the heat exchange with the surroundings are properly captured in the model.

The model is based on the following assumptions:

- The thickness of the plate is assumed to be much smaller than its radius
  ($s \ll R$).
- The temperature distribution follows radial symmetry, so angular variation is neglected.
- Thermal diffusivity, density, and specific heat capacity are assumed to remain uniform during the simulation and do not change with temperature. This assumption gives a constant value of thermal diffusivity.
- The material of the plate is considered homogeneous and isotropic.
- According to Newton's law of cooling, heat loss is proportional to the temperature difference, but the law has certain limits. In this study, h (the convection heat transfer coefficient) is assumed constant, while in reality it changes with temperature, and the law is accurate only for small temperature differences.
- The ambient temperature is assumed to remain constant throughout the simulation.
- The effects of thermal expansion and mechanical stress on heat transfer are neglected.
- Heat transfer by thermal radiation is considered negligible compared to convection and conduction.
- The Gaussian source at the center is considered time-independent and constant during the simulation.

2.2 Gaussian Heat Source

The thermal energy applied within the plate is depicted by a Gaussian distribution that radiates outward.

$$Q(r) = Q_0 e^{-\beta r^2}$$

An increased value of β causes the heat to concentrate more tightly around the center, whereas a decreased value disperses the heat more widely across the plate, leading to a reduction in intensity. Thus, the parameter β regulates whether the heating effect is focused or distributed.This category of

heat source possesses two primary characteristics. Firstly, it is contingent upon the radial distance r from the center, indicating that the heating is at its peak when r=0 and diminishes progressively as r increases. Secondly, for the purposes of this study, it is considered to be time-independent, ensuring that the heating profile remains uniform during the entire simulation.

A Gaussian profile is chosen here because it gives a smooth and realistic way to represent localized energy input, such as from a focused laser beam or a small central heater. Unlike an ideal point source, the Gaussian does not create mathematical singularities at the center and is easier to handle in numerical simulations. It also provides flexibility to control both the intensity and the spread of heating through the parameters Q_0 and β.

Since this source term represents a real energy input (with units of $\mathrm{W/m^3}$), it is divided by the areal heat capacity ρcs in the governing equation. This ensures that its effect is expressed as a temperature rise rate (K/s), consistent with the thermal behavior of the plate.

2.3 Model Conditions

For the mathematical model to be well-defined, it is essential to specify both an initial condition and appropriate boundary conditions. The initial condition characterizes the thermal state of the plate at the beginning of the process, while the boundary conditions govern the heat exchange at the plate's edges throughout the simulation.

Initial Condition: At time t=0, the plate is assumed to be at the ambient temperature everywhere. This represents the physical case where, before heating begins, the plate is in thermal balance with its surroundings. Mathematically, this is expressed as

$$u(r, 0) = T_\infty, \quad 0 \leq r \leq R$$

This condition provides a uniform starting point for the system's temperature evolution.

Condition at the center: Since both the geometry and the heating are symmetric about the center of the plate, there is no preferred direction for heat flow at r=0. As a result, the temperature gradient at the origin

must be zero. This leads to the boundary condition

$$\frac{\partial u}{\partial r}(0,t) = 0, \quad t > 0$$

This condition ensures that no artificial heat flux appears at the center and that the solution stays smooth and physically consistent.

Condition at the rim: At the outer boundary, $r{=}R$, the plate loses heat to the surrounding air. This process is modeled using Newton's law of cooling, which states that the heat flux at the boundary is proportional to the difference between the plate temperature and the ambient temperature. This leads to the following Robin boundary condition.

$$-k\frac{\partial u}{\partial r}(R,t) = h\big(u(R,t) - T_\infty\big), \quad t > 0$$

The left-hand side of the condition represents the conductive heat flux at the boundary, while the right-hand side represents the convective heat loss to the surroundings. Together, they express the balance of energy at the plate's edge.

2.4 Discretization of the Domain

To solve partial differential equations numerically, the continuous problem must be converted into a finite set of algebraic equations that a computer can handle. This process is called discretization. Since digital computers can only work with a limited number of points and with finite precision, both space and time are divided into small steps. In this way, the original infinite-dimensional problem is reduced to a finite system that can be solved numerically.

Spatial discretization: The radial domain of the circular plate, $0 \leq r \leq R$, is divided into N sub-intervals of uniform length.

$$\Delta r = \frac{R}{N}.$$

This creates a structured mesh of $N + 1$ points defined as

$$r_i = i\Delta r, \quad i = 0, 1, 2, \ldots, N,$$

where $r_0 = 0$ represents the center of the plate, $r_N = R$ represents the outer rim, and the intermediate values $r_1, \ldots, r_{N-1}$ are the interior mesh

points. A uniform mesh is chosen to simplify the use of standard finite-difference formulas and to keep the error behavior consistent across the computational domain. It should also be noted that finite-difference approximations always introduce some error, since they replace continuous derivatives with discrete estimates.

Temporal discretization: The time domain $[0, T_{\max}]$ is partitioned into uniform steps of size Δt. The discrete time levels are given by

$$t^n = n\Delta t, \quad n = 0, 1, 2, \ldots, M,$$

where

$$M = \frac{T_{\max}}{\Delta t}$$

is the total number of time steps required to reach the final simulation time. The superscript n is used throughout to indicate the discrete-time level.

The continuous temperature field $u(r, t)$ is now expressed through discrete values established at the mesh points, denoted as $u_i^n \approx u(r_i, t_n)$. In this context, the subscript i indicates the spatial position along the radius, whereas the superscript n indicates the time level. Consequently, the temperature is no longer regarded as a continuous function but rather as a set of values arranged on a two-dimensional grid in both space and time, which serves as the foundation for the subsequent numerical scheme.

2.5 Finite-Difference Approximation

In order to numerically solve the governing partial differential equation, the time and space derivatives are substituted with approximate formulas based on the discrete mesh previously described. The selection of finite-difference formulas affects the accuracy, stability, and efficiency of the method. In this research, the time derivative is estimated using a forward difference, whereas the spatial derivatives in the radial direction are estimated using central differences.

The time derivative is expressed through the forward difference formula, which serves as the foundation for the explicit time-stepping method:

$$\frac{\partial u}{\partial t}(r_i, t^n) \approx \frac{u_i^{n+1} - u_i^n}{\Delta t}$$

This first-order approximation estimates the temporal rate of change by comparing the present temperature with its future value at the next time level. Its use allows the explicit scheme to compute unknown values directly from previously known data.

For the spatial derivatives in the radial coordinate, second-order central differences are applied. The first derivative is given by

$$\frac{\partial u}{\partial r}(r_i, t^n) \approx \frac{u_{i+1}^n - u_{i-1}^n}{2\,\Delta r}$$

and the second derivative is approximated by the standard three-point stencil

$$\frac{\partial^2 u}{\partial r^2}(r_i, t^n) \approx \frac{u_{i+1}^n - 2u_i^n + u_{i-1}^n}{(\Delta r)^2}.$$

These formulas are applied at interior mesh points, where both neighboring values are available.

To compute the radial derivative at the outer boundary, it is necessary to use a one-sided finite-difference approximation due to the unavailability of values beyond the domain. In this work, a first-order backward difference method is adopted,

$$\frac{\partial u}{\partial r}(r_N, t^n) \approx \frac{u_N^n - u_{N-1}^n}{\Delta r},$$

This formula gives a proper way to represent the derivative at the outer edge of the plate without the need to add extra points outside the domain. Even though it is only first–order accurate, it works well for applying the Robin boundary condition and is often used in explicit methods.

An important feature of the radial heat equation is the composite term

$$u_{rr} + \frac{1}{r}u_r,$$

which seems to become singular at the center of the plate ($r = 0$). This difficulty is resolved by applying the physical symmetry condition $u_r(0, t) = 0$ by using Taylor expansion of $u(r, t)$ around the origin. The expansion shows that the combination $u_{rr} + \frac{1}{r}u_r$ has a finite and well-defined limit as $r \to 0$, namely

$$\lim_{r\to 0}\left(u_{rr} + \frac{1}{r}u_r\right) = 2u_{rr}(0, t).$$

At the discrete level, this limit is represented by the finite-difference relation

$$\left(u_{rr} + \frac{1}{r}u_r\right)\Big|_{r=0} \approx \frac{2}{(\Delta r)^2}\left(u_1^n - u_0^n\right).$$

This approach removes the division by zero, enforces the natural symmetry at the plate centre, and provides a consistent second-order approximation.

2.6 Application to the Governing Equation

Using the finite-difference formulas described earlier, the original heat conduction equation is rewritten in a form that can be applied directly on the grid. In this way, the continuous problem is reduced to a set of update relations for the temperature values at each mesh point and time step.

At the interior mesh points r_i $(1 \leq i \leq N-1)$, inserting the forward difference for time and the central differences for space gives the explicit update scheme.

$$\frac{u_i^{n+1}-u_i^n}{\Delta t} = \alpha \left[\frac{u_{i+1}^n - 2u_i^n + u_{i-1}^n}{(\Delta r)^2} + \frac{1}{r_i} \cdot \frac{u_{i+1}^n - u_{i-1}^n}{2\Delta r} \right] + \frac{Q_0 e^{-\beta r_i^2}}{\rho c s} - \frac{2h}{\rho c s}(u_i^n - T_\infty)$$

After rearranging, the formula provides the updated temperature u_i^{n+1} for the next time level.

$$\boxed{u_i^{n+1} = u_i^n + \Delta t \left\{ \alpha \left[\frac{u_{i+1}^n - 2u_i^n + u_{i-1}^n}{(\Delta r)^2} + \frac{1}{r_i} \cdot \frac{u_{i+1}^n - u_{i-1}^n}{2\Delta r} \right] + \frac{Q_0 e^{-\beta r_i^2}}{\rho c s} - \frac{2h}{\rho c s}(u_i^n - T_\infty) \right\}}$$

This update shows that the new temperature at node i depends directly on the three neighboring values u_{i-1}^n, u_i^n, and u_{i+1}^n of the previous time step. This relationship is illustrated in the stencil diagram, where the red point at time level $n+1$ is connected to its three supporting black points at time level n.

The explicit update for the center node ($r = 0$), after removing the singularity, is given by

$$\boxed{u_0^{n+1} = u_0^n + \Delta t \left\{ \alpha \left[\frac{2(u_1^n - u_0^n)}{(\Delta r)^2} \right] + \frac{Q_0 e^{-\beta r_i^2}}{\rho c s} - \frac{2h}{\rho c s}(u_0^n - T_\infty) \right\}}$$

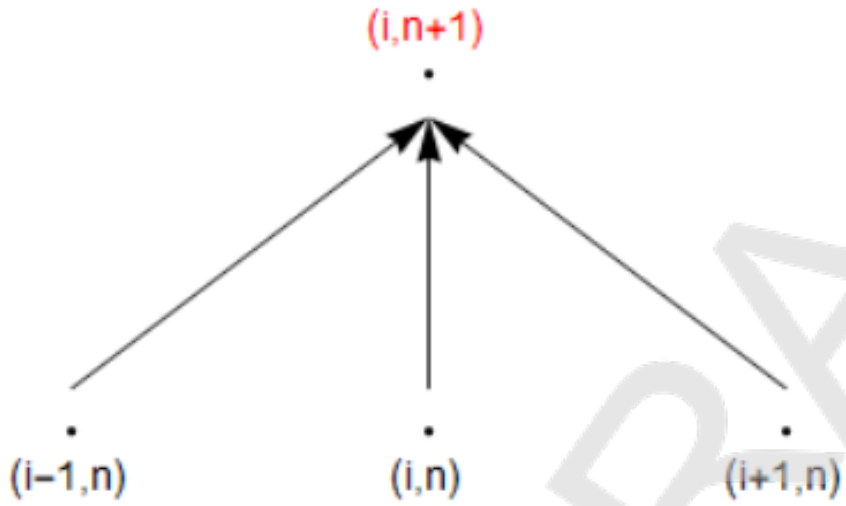

Figure 1: **Interior-node stencil**

At the center of the plate, the symmetry condition removes the singularity, so the update depends only on the center value u_0^n and its immediate neighbor u_1^n. This is reflected in the stencil diagram, where the red node at level $n+1$ depends only on these two supporting nodes from the previous time step.

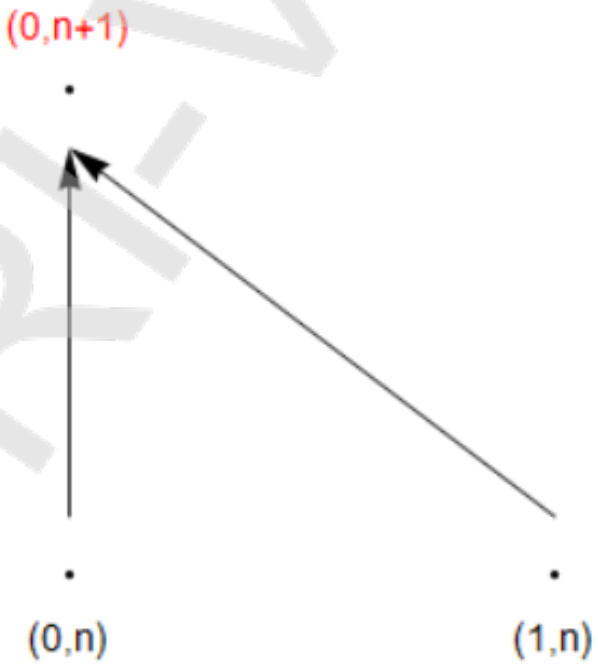

Figure 2: **Centre-node stencil**

At the outer boundary $r_N = R$, the finite-difference evaluation of the

derivative would typically need an external point (r_{N+1}), known as a ghost point. Instead of introducing such an artificial value, the Robin boundary condition is applied at the rim, and the derivative is approximated with a one-sided (backward) difference. The heat conducted to the edge of the plate is required to balance the convective heat flux leaving to the environment. This relation is expressed as Robin boundary condition.

$$-k\frac{\partial u}{\partial r}(R,t) = h\big(u(R,t) - T_\infty\big)$$

Substituting one-sided backward difference into this condition gives

$$-k\frac{u_N^n - u_{N-1}^n}{\Delta r} = h\left(u_N^n - T_\infty\right)$$

Rearranging yields the relation

$$\boxed{u_N^n = \frac{u_{N-1}^n + \frac{h\Delta r}{k}T_\infty}{1 + \frac{h\Delta r}{k}}}$$

At the rim, the Robin boundary condition eliminates the need for a ghost point by combining the interior neighbor u_{N-1}^n with the ambient temperature T_∞. The stencil diagram illustrates this condition.

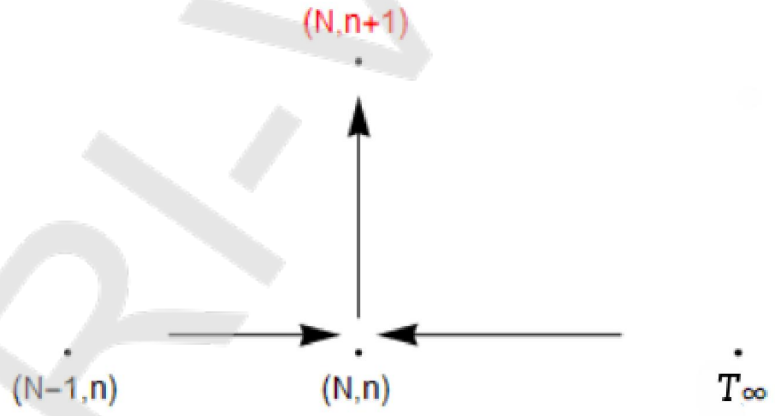

Figure 3: **Rim-node stencil**

This equation serves two purposes. First, it shows that heat transfer at the rim is governed by convection into the surrounding medium. Second, it removes the need for a ghost point outside the domain, thereby closing the system of equations on the defined mesh. At each time step, this condition provides the rim temperature directly from the adjacent interior value and the ambient temperature.

2.7 Stability Analysis of the Explicit Scheme

The explicit finite-difference scheme is conditionally stable, which means that the time step must be restricted in order to prevent the growth of errors. If the time step is too large, even very small round-off or discretization errors will grow over time, causing the numerical solution to become unstable. To understand the limits on the time step, we use a method called von Neumann stability analysis.

Von Neumann stability analysis: The von Neumann method studies how small errors evolve when the numerical scheme is applied step after step. Suppose that during the computation a very small error arises at each grid location. This error at node i and time level n is denoted by ε_i^n, meaning the error value corresponding to node i at step n. We then assume this error has the form of a Fourier wave:

$$\varepsilon_i^n = G^n e^{ikr_i}$$

Here, $r_i = i\Delta r$ is the spatial position of node i, k is the wavenumber of the Fourier mode, and G is called the *amplification factor*. This assumption does not impose any restriction, since any error distribution can be represented as a combination of Fourier modes. Stability of the scheme is ensured if none of these modes grow in time. Accordingly, the requirement for stability is that the amplification factor satisfies $|G| \leq 1$ for all modes.

The 1D heat equation as a reference case: To get an idea of stability, we first consider a simpler method before applying the analysis to the full equation. Consider the simple one-dimensional heat equation $u_t = \alpha u_{xx}$, where α is the thermal diffusivity. Using the forward-time, centered-space (FTCS) scheme, we write

$$\frac{u_i^{n+1} - u_i^n}{\Delta t} = \alpha \frac{u_{i+1}^n - 2u_i^n + u_{i-1}^n}{(\Delta r)^2}.$$

Substituting the Fourier error mode into this update equation and simplifying, we find the amplification factor:

$$G = 1 - 4\lambda \sin^2\left(\frac{\theta}{2}\right),$$

where

$$\lambda = \frac{\alpha \Delta t}{(\Delta r)^2}, \quad \theta = k\Delta r.$$

The most restrictive case occurs when $\theta = \pi$, giving $G = 1 - 4\lambda$. To ensure $|G| \leq 1$, we require

$$\lambda \leq \frac{1}{2}.$$

Thus, the maximum allowable time step in this case is

$$\Delta t \leq \frac{(\Delta r)^2}{2\alpha}.$$

This approach is used to analyze stability in numerical methods through von Neumann analysis, where errors are treated as Fourier waves. We now apply this method to the equation considered in the present work.

The axis-symmetric heat equation: The operator that governs the present formulation can be expressed as

$$u_t = \alpha \left(u_{rr} + \frac{1}{r} u_r \right).$$

At the interior points, where $r > 0$, the term $(1/r)u_r$ works as a smaller correction compared to the main diffusion part of the equation, and therefore it does not change the stability limit in any major way. The stability condition is still mainly controlled by the diffusion term.

At the centre point $r = 0$, the situation is different. Due to symmetry, we impose the condition $u_r(0, t) = 0$. By expanding the solution in a Taylor series around the origin, we obtain the following relation:

$$\lim_{r \to 0} \left(u_{rr} + \frac{1}{r} u_r \right) = 2u_{rr}(0, t)$$

This result shows that the second derivative at the centre is effectively twice its usual value. In the discrete scheme, this doubles the diffusion term in the update formula for the centre node. Consequently, the stability limit is reduced by half.

$$\Delta t \leq \frac{(\Delta r)^2}{4\alpha}$$

As a result, the stability restriction at the centre node is more stringent than in the reference case of the 1D heat equation.

At the plate faces, convective cooling to the surrounding air is represented by a distributed sink term of the form

$$-\Gamma\big(u - T_\infty\big), \quad \Gamma = 2h/\rho cs,$$

For the simple ODE $u_t = -\Gamma u$, forward Euler integration is stable if

$$0 \leq \Gamma \, \Delta t \leq 2.$$

This gives another restriction on the time step:

$$\Delta t \leq \frac{2}{\Gamma}.$$

Taking into account both the diffusion limit at the center node and the convective boundary at the rim, the numerical scheme is stable, provided that

$$\Delta t \leq \min\left(\frac{(\Delta r)^2}{4\alpha}, \frac{2}{\Gamma}\right)$$

For practical purposes, computations are performed conservatively, with a safety factor applied to ensure that the dimensionless number $\lambda = (\alpha \, \Delta t)/(\Delta r)^2$ satisfies $\lambda \leq 0.20$, ensuring robust numerical behavior even if other approximations or rounding errors are present.

3 Numerical Application

We are starting the numerical application by taking a numerical setup of an illustrative example. The case will be analyzed through different plots to demonstrate the behavior of the explicit scheme. We consider the plate material to be gold. All the values chosen for geometry, material properties, heat source and numerical parameters are mentioned below.

Geometrical parameters	
Plate radius	$R = 0.10$ m
Plate thickness	$s = 0.005$ m
Material properties (Gold)	
Thermal conductivity	$k = 318$ W/(m · K)
Density	$\rho = 19{,}300$ kg/m^3
Specific heat	$c = 129$ J/(kg · K)
Thermal diffusivity	$\alpha = 1.28 \times 10^{-4}$ m^2/s
Heat transfer parameters	
Ambient temperature	$T_\infty = 293$ K
Convective coefficient	$h = 25$ W/(m^2 · K)
Distributed sink term	$\Gamma = \dfrac{2\,h}{\rho\,c\,s}$
Heat source parameters	
Source amplitude	$Q_0 = 2.0 \times 10^5$ W/m^3
Spread parameter	$\beta = 4.0 \times 10^6$ m^{-2} (0.5 mm width)
Numerical discretization	
Number of radial intervals	$N = 400$
Radial step size	$\Delta r = 2.5 \times 10^{-4}$ m
Time step	$\Delta t = 0.88 \times 10^{-4}$ s (with $\lambda = 0.18$)
Total simulation time	600 s
Number of steps	6812065

Table 2: Parameters used in the numerical setup.

To interpret the numerical results, several graphical illustrations are presented. These include temperature variation with time at selected radii, radial profiles at fixed times, a space–time heatmap with contours, and heat flux distributions. Together, they provide a clear picture of the thermal response of the plate under Gaussian heating with convective cooling.

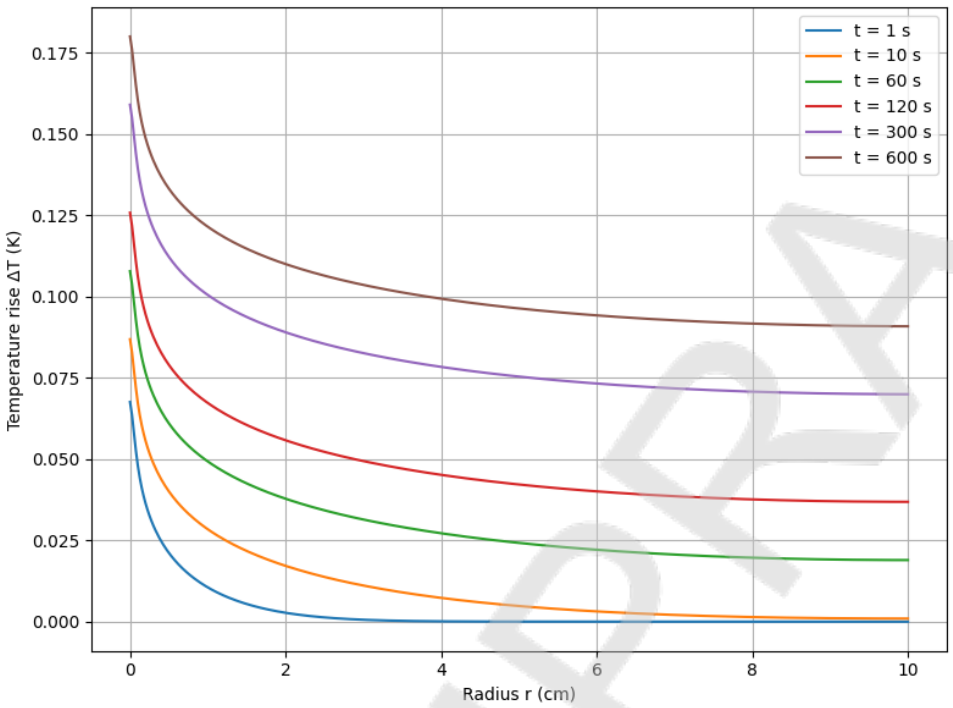

Figure 4: **Radial temperature profiles at different times**

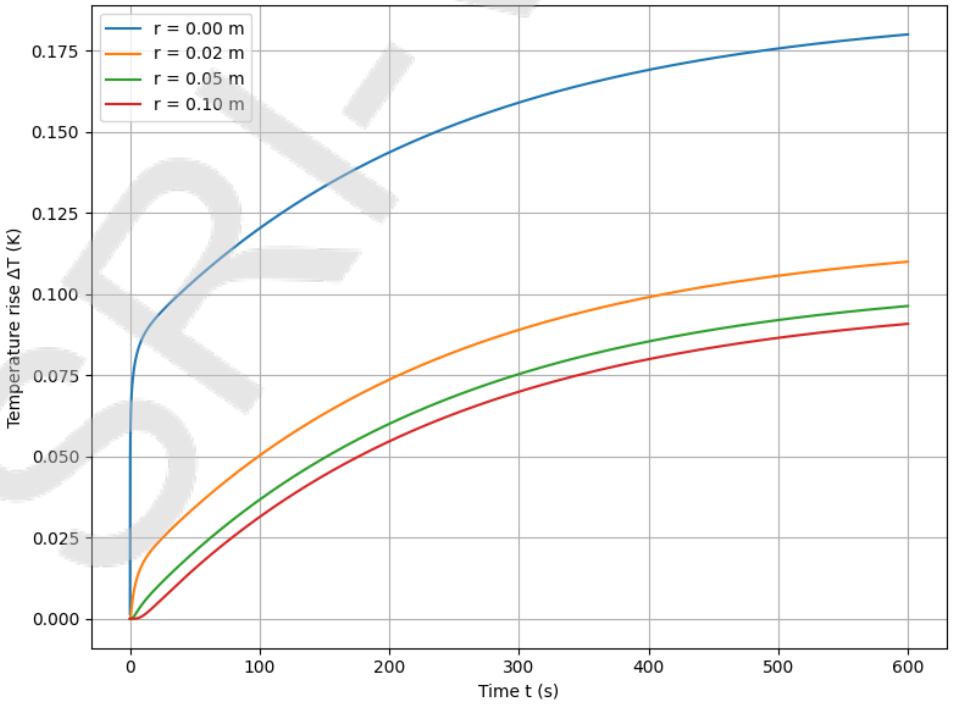

Figure 5: **Temperature rise versus time at selected radii**

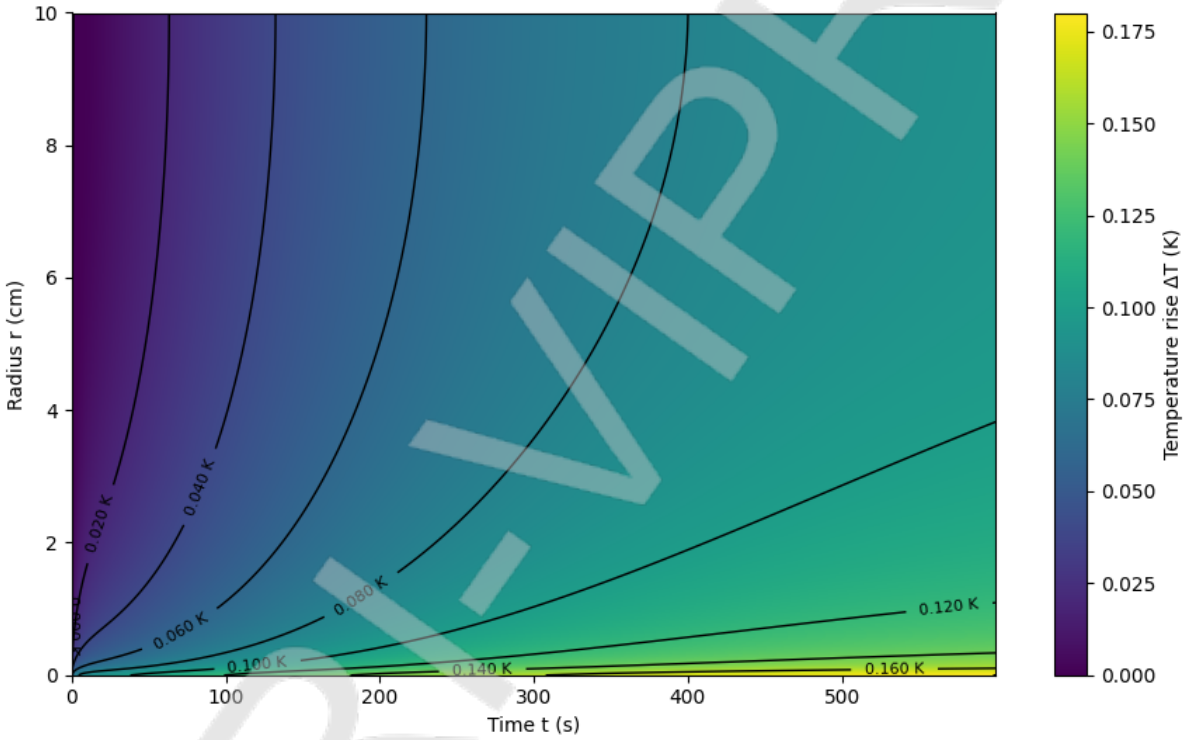

Figure 6: **Space–time map of temperature rise with contour lines**

The simulations show a stable and realistic thermal response of the circular plate. The center experiences the largest temperature rise because of the Gaussian heat source, while the temperature decreases smoothly toward the rim. Over time, the sharp gradients reduce as heat spreads outward and convection balances the input. The rise stays very small (less than one degree), which agrees with expectations for a highly conductive gold plate cooled by natural air convection. The curves and heatmap remain smooth without unwanted oscillations, confirming that the explicit FTCS scheme is used within its stability range ($\lambda = 0.18 < 0.20$). The added face-loss term also works well and does not reduce accuracy. Overall, the results are both stable and physically meaningful, showing that the chosen model and parameters are valid.

(The simulations presented here were carried out using an in-house Python implementation of the explicit FTCS scheme with Gaussian heating and convective losses. The complete simulation code can be shared by the corresponding author on request.)

4 Conclusion

In this study, transient heat conduction in a thin circular plate under a Gaussian heat source and convective cooling were simulated using the explicit FTCS scheme. The method was found to work reliably within the stability limits, although it required a very fine mesh and many time steps to maintain accuracy. Despite these computational requirements, the results were physically consistent and captured the expected temperature response of the plate. The main limitation of the explicit method is its restrictive time-step condition, which suggests the use of more advanced techniques. In future work, semi-implicit or fully implicit approaches, such as the Crank-Nicolson method, can be explored, as they offer improved stability and efficiency for solving such problems while preserving accuracy.

References

[1] HS Carslaw and JC Jaeger. Conduction of heat in solids, clarendon, 1959.

[2] Jean Baptiste Joseph Baron Fourier et al. *The analytical theory of heat*. Courier Corporation, 2003.

[3] Lawrence C Evans. *Partial differential equations*, volume 19. American mathematical society, 2022.

[4] RL Herman. Numerical solution of 1d heat equation. 2014.

[5] Mohammad A Saraireh. Thermal performance of heat conduction in a square plate. *International Journal of Simulation–Systems, Science & Technology*, 18(4), 2017.

[6] M Necati Özışık. *Heat conduction*. John Wiley & Sons, 1993.

[7] BA Peavy. Steady state heat conduction in cylinders with multiple continuous line heat sources. *J Res Natl Bur Stand C Eng Instrum*, 67(2):119–28, 1963.

[8] Gordon D Smith. *Numerical solution of partial differential equations: finite difference methods*. Oxford university press, 1985.

[9] Jae-Yuh Lin and Han-Taw Chen. Radial axisymmetric transient heat conduction in composite hollow cylinders with variable thermal conductivity. *Engineering analysis with boundary elements*, 10(1):27–33, 1992.

[10] SV Patankar. Patankar numerical heat transferand fluid flow. 1980.

[11] Steven C Chapra, Raymond P Canale, et al. *Numerical methods for engineers*, volume 1221. Mcgraw-hill New York, 2011.

[12] John Conrad Jaeger. Moving sources of heat and the temperature at sliding contacts. *Proc. Roy. Soc. New South Wales*, 76:203, 1942.

[13] David G Cahill, Wayne K Ford, Kenneth E Goodson, Gerald D Mahan, Arun Majumdar, Humphrey J Maris, Roberto Merlin, and Simon R Phillpot. Nanoscale thermal transport. *Journal of applied physics*, 93(2):793–818, 2003.

[14] John Pearce. Mathematical models of laser-induced tissue thermal damage. *International Journal of Hyperthermia*, 27(8):741–750, 2011.

[15] John Crank and Phyllis Nicolson. A practical method for numerical evaluation of solutions of partial differential equations of the heat-conduction type. In *Mathematical proceedings of the Cambridge philosophical society*, volume 43, pages 50–67. Cambridge University Press, 1947.